

1 Diverse sensitivity of winter crops over the growing season to climate and land
2 surface temperature across the rainfed cropland-belt of eastern Australia

3
4 Jianxiu Shen ^{a,*}, Alfredo Huete ^b, Ngoc Nguyen Tran ^b, Rakhesh Devadas ^b, Xuanlong Ma ^b,
5 Derek Eamus ^a, Qiang Yu ^{a,c,d}

6 ^a School of Life Sciences, University of Technology Sydney, NSW 2007, Australia

7 ^b Climate Change Cluster, University of Technology Sydney, NSW 2007, Australia

8 ^c State Key Laboratory of Soil Erosion and Dryland Farming on the Loess Plateau, Northwest
9 A&F University, Yangling 712100, China

10 ^d College of Resources and Environment, University of Chinese Academy of Science, Beijing
11 100049, China

12 * Corresponding author (Jianxiu.Shen@student.uts.edu.au)

13

14

15 ABSTRACT

16 The rainfed cropland belt in Australia is of great importance to the world grain market but has the
17 highest climate variability of all such regions globally. However, the spatial-temporal impacts of
18 climate variability on crops during different crop growth stages across broadacre farming systems
19 are largely unknown. This study aims to quantify the contributions of climate and Land Surface
20 Temperature (LST) variations to the variability of the Enhanced Vegetation Index (EVI) by using
21 remote sensing methods. The datasets were analyzed at an 8-day time-scale across the rainfed
22 cropland of eastern Australia. First, we found that EVI values were more variable during the crop
23 reproductive growth stages than at any other crop life stage within a calendar year, but
24 nevertheless had the highest correlation with crop grain yield ($t\ ha^{-1}$). Second, climate factors and
25 LST during the crop reproductive growth stages showed the largest variability and followed a
26 typical east-west gradient of rainfall and a north-south temperature gradient across the study area
27 during the crop growing season. Last, we identified two critical 8-day periods, beginning on day
28 of the year (DoY) 257 and 289, as the key ‘windows’ of crop growth variation that arose from the
29 variability in climate and LST. Our results show that the sum of the variability of the climate
30 components within these two 8-day ‘windows’ explained >88% of the variability in the EVI, with
31 LST being the dominant factor. This study offers a fresh understanding of the spatial-temporal
32 climate-crop relationships in rainfed cropland and can serve as an early warning system for
33 agricultural adaptation in broadacre rainfed cropping practices in Australia and worldwide.

34

35 KEY WORDS

36 Climate variability; MODIS EVI; crop growth stages; land surface temperature; rain-fed
37 croplands; eastern Australia

38

39 1 INTRODUCTION

40 As the world's fourth largest agriculture exporter, Australia, whose crop production accounts for
41 over 13% of its export revenue (ABARES, 2017), has greatly influenced the world grain market
42 in recent decades (Hamblin 2009; Lawrence et al. 2013). Due to the interactions of three oceans,
43 the Australian climate has the greatest variability among inhabited continents (Cleverly et al.
44 2016; Ma et al. 2016; Stokes & Howden 2010; Xie et al. 2016). Rainfall, air temperature and
45 solar radiation are direct growth-defining and limiting factors of broadacre crops (Yu et al. 2001),
46 and their variability poses risks to Australian crop production in terms of reductions in harvest
47 area (Cohn et al. 2016) and grain yield (Barlow et al. 2015; Zheng et al. 2012) as well as changes
48 to the dates that define the crop growing season (Zheng et al. 2012). Recent studies have shown
49 that Australian croplands, which are mostly characterized by a broadacre rainfed planting system,
50 are vulnerable in grain production to current climate variability (Field et al. 2014; Tripathi et al.
51 2016). While the projected growth of the global human population necessitates an increased crop
52 yield (Godfray et al. 2010; Hochman et al. 2017), growth in annual grain yield in Australia has
53 stalled since 1990, which is majorly caused by the changing climate (Hochman et al. 2017). Thus,
54 it is necessary to quantify the impacts of climate variability on crop growth and to take measures
55 to enhance the development of agricultural early warning systems.

56 Climate-crop relationships have been intensively researched in recent decades. Based on a recent
57 study, climate variation is responsible for approximately one-third (~32–39%) of global variation

58 in crop yield (Ray et al. 2015). In Australia, climate variation in the state of New South Wales
59 (NSW) accounted for 31–47% of inter-annual wheat yield from 1922 to 2000 (Wang, Chen, et al.
60 2015). The results of crop simulations (Asseng et al. 2011) have indicated that variations of 2°C
61 of the average temperature during the crop growing season can cause up to a 50% reduction in
62 grain production in Australian croplands. Under projected future climate scenarios, wheat yield
63 will decrease by approximately 25% because of the predicted increase of temperature in
64 southeastern Australia in future decades (Anwar et al. 2007). In most previous studies, the
65 approaches of climate-crop relationship can be divided into two major types: observational and
66 statistical models, and crop simulation techniques. The observational and statistical models have
67 been based on data collected from administrative boundaries, which do not reflect the
68 crop-growing process and do not explicitly reflect the spatial relationships identified. Although
69 crop simulation techniques can precisely reconstruct the growth cycles of crops using parameter
70 pre-setting, it is labor intensive to spatially up-scale the simulations from the field plot to
71 ecosystem or regional scales (Rosenzweig et al. 2013). This is due to the fact that crop simulation
72 needs considerable efforts in data collection and parameter calibration to overcome its limitations
73 in spatial heterogeneity.

74 These limitations in spatial up-scaling can be overcome by introducing remote sensing detection
75 methods (Reed et al. 1994; Sakamoto et al. 2005) or by combining crop models with satellite
76 observations (Ma et al. 2008; Moulin et al. 1998). Satellite radiometric observations offer the
77 advantage of multiple spatial, temporal and spectral resolutions and the data are from real-time
78 observations (Eamus et al. 2016), which can characterize the full profile of the vegetation growth
79 cycle. Remote sensing methods that have been utilized for crop-climate relationships often focus
80 on estimating the cropland area (Biradar et al. 2009; Potgieter et al. 2011; Wardlow & Egbert

81 2008) and detecting vegetation green-up and green-fade dates (Guo et al. 2016; Sakamoto et al.
82 2013). However, every stage of the crop growth cycle can impact the final crop yield. Currently,
83 there is little knowledge about the different responses of crop performance to regional climate
84 variability at each growth stage.

85 Understanding the impacts of climate on crop growth over its life span can help farmers and
86 agricultural departments make timely decisions in response to climate variability and reduce
87 potential losses in yield (Rabbinge 2007) in broadacre rainfed cropping systems in Australia and
88 worldwide. Thus, there is a need to illustrate the relationships between variations in several
89 climate factors and crop growth throughout all crop growth stages and to identify the most
90 sensitive 'windows', that is, the time segments of crop-growth that are most sensitive to climate
91 variability.

92 Vegetation Indexes (VIs) are widely used remote indicators that characterize the status of land
93 surface vegetation as well as the biophysical properties on global and regional scales (Karnieli et
94 al. 2010; Wan et al. 2004). The VIs measure the 'greenness' of the canopy and monitor vegetation
95 growth and health at various spatial scales (Huete et al. 2002; Ma et al. 2015). The Enhanced
96 Vegetation Index (EVI) used in this study is an optimized VI that can effectively reduce soil
97 background and atmospheric effects (Huete et al. 2002; Huete 2012; Suepa 2013).

98 Rainfall, air temperature and radiation influence crop canopy greenness by directly and indirectly
99 controlling crop transpiration and photosynthesis (Calzadilla et al. 2013; Eamus et al. 2016)
100 within the soil-plant-atmosphere continuum. Both the vegetative growth and reproductive growth
101 stages of crops are dependent on and affected by these factors. The direct effects of variations in
102 these factors on crop growth can be dominant during different growth stages. However, the
103 proportion of the indirect effects of the complex interactions among these factors (Yu et al. 2014)

104 on crops cannot be explained without a comprehensive indicator of the crop water and heat status.
105 The radiative canopy temperature, (the Land Surface Temperature (LST)), is designed to measure
106 the physical processes of the ground surface energy and water balance (Li et al. 2013) and
107 reflects the water and heat status of vegetation and soil. In most cases, a high LST indicates
108 deficient soil moisture and a high canopy heat stress (Karnieli et al. 2010). Thus, we introduced
109 LST as a potentially crop-limiting climate component to describe the indirect impacts of rainfall,
110 air temperature and solar radiation on crop growth.

111 This study investigated regional inter-annual variations in climate-crop growth relationships by
112 incorporating MODIS land cover maps, time-series Enhanced Vegetation Index (EVI) and Land
113 Surface Temperature (LST) products, ground meteorological station data and *in-situ* trial data
114 across the rainfed cropland belt in NSW during the period from 2001 to 2013. An 8-day
115 time-scale is applied as this is the attainable time step for the satellite that provides the data to
116 produce MODIS EVI and LST. The objectives of this study are to: (1) identify the seasonality,
117 trends and variability for EVI and each climate component during the crop growing season; (2)
118 evaluate the individual and collective impacts of climate and LST variability on crops at the pixel
119 and regional levels; and (3) investigate the relative contribution of the variability of each climate
120 component to variation in crop growth during each 8-day time segment.

121

122 2 MATERIALS AND METHODS

123 2.1 Study area

124 The land cover map used in this study was obtained from the Dynamic Land Cover Dataset
125 (DLCD) for Australia (<http://www.ga.gov.au/>) developed by Geoscience Australia. This dataset

126 is based on an analysis of a 16-day MODIS EVI composite at a 250-meter resolution during
127 2000-2008 (Lymburner et al. 2010). The dataset distinguishes rainfed cropland from irrigated
128 cropland in Australia and shows a high degree of consistency (93%) with extensive independent
129 field-based investigations.

130 `## Figure 1 insert here##`

131 Australian rainfed croplands (Figure 1a) extend over 24.6 million hectares in a crescent around
132 eastern, southern and western Australia and produce approximately 22.9 million tons of grain per
133 year (www.abares.gov.au, 2013). Wheat is the major agriculture commodity across the rainfed
134 cropland belt in Australia (Hochman et al. 2017). The NSW cropland belt (Figure 1b) stretches
135 across the drier western face of the Australian Great Dividing Range. It accounts for 27.5% of the
136 wheat planted area in Australia and 27% of the total wheat production of the nation
137 (www.abares.gov.au, 2013-14), which makes NSW the second-highest wheat producing state in
138 Australia. The NSW wheat belt (Figure 1c) has an average elevation of 287.8 m and a gradient of
139 50 to 750 m from west to east. The annual wheat production during the period from 2003 to 2014
140 varied between 2.48 and 10.49 million tons, and the yield varied by approximately 5-fold
141 ($0.62\text{--}2.75\text{ t ha}^{-1}$) (www.abares.gov.au, 2013-14). Historically, wheat production in NSW has
142 shown vulnerability to climate variability due to high exposure to water and heat stresses (Wang,
143 Liu, et al. 2015). The mean annual air temperature and rainfall across the entire cropland belt of
144 NSW vary between 12–20°C and 250–800 mm, respectively, highlighting the significant spatial
145 variation in climate conditions and revealing the complexity of modelling crop yields across
146 broad spatial extents.

147

148 2.2 Data processing

149 2.2.1 Meteorological data and study sites

150 The meteorological station-based observational data from the Scientific Information for Land
151 Owners (SILO) patched point dataset (<http://www.bom.gov.au/silo/>) for NSW were collected,
152 and we extracted 161 study sites that were identified as being located in rainfed cropland pixels;
153 both their ground meteorological data and spatially observed data were available. These sites are
154 evenly distributed across our study area (Figure 1b). As climate-driving parameters, daily rainfall
155 (Rain), maximum air temperature (T_{\max}), minimum air temperature (T_{\min}), and solar radiation
156 (Radn) from 2000 to 2014 were extracted for each site. We then up-scaled them to an 8-day time
157 series to remove outliers and noise as well as to match the temporal resolution with remote
158 sensing datasets. We averaged the 8-day Rain, T_{\max} , T_{\min} and Radn from the 161 sites to represent
159 the generalized climate patterns of the time series across the NSW wheat belt.

160

161 2.2.2 Remote sensing and *in-situ* datasets

162 Approximately 14 years (February 2000–December 2014) of 16-day Terra-MODIS EVI data
163 (MOD13A1) at a spatial resolution of 500 meters and of 8-day Terra-MODIS LST
164 (MOD11A2_day) with a 1000-meter resolution were obtained online from the NASA Land
165 Processes Distributed Active Archive Center (LP DAAC). The original data were then filtered
166 based on the Quality Control layers along with the MOD13A1 and MOD11A2_day data. To
167 unify the spatial and temporal resolutions of these 2 remote sensing datasets, the EVI values were
168 interpolated and filled to achieve an 8-day series using the spline method, and the LST were

169 resampled to a 500-meter spatial resolution (Broich et al. 2015). Time-series profiles of the 500
170 m EVI and LST for the selected 161 cropland pixels were then extracted.

171 The integrated EVI (iEVI) has been widely used to represent vegetation productivity (Ma et al.
172 2015; Ponce Campos et al. 2013), which refers to the area under the EVI curve in a growing
173 season. Here, we used iEVI to illustrate the spatial variation of accumulated aboveground
174 biomass during the growing season. The iEVI and average climate conditions during the crop
175 growing season at each selected pixel were calculated and interpolated using the inverse distance
176 weighting (IDW) interpolation method over the study area.

177 The *in-situ* wheat trial (2005–2013) datasets were obtained from the Grains Research and
178 Development Corporation (GRDC) National Variety Trials (NVT), Australia
179 (<http://www.nvtonline.com.au/>). The sowing date, harvest date, and actual yield of separate
180 groups of wheat trials for each year from 2005 to 2013 were recorded. There were 117 trial sites
181 collected in total, and they were evenly distributed across the NSW croplands.

182

183 2.2.3 Phenology metrics detection

184 We discriminated the green-up (start of season, SOS), green-fade (end of season, EOS) and peak
185 dates (peak of season, POS) of the growing season from the 8-day MODIS EVI time series
186 profile using the following rules: (i) daily EVIs were reconstructed by using the
187 Polyfit-Maximum method (Cong et al. 2013; Piao et al. 2006) with a degree of 9; (ii) the
188 inflection point of the maximum of the second derivative during winter (from May to August)
189 was identified as the SOS (Gong et al. 2015), while another inflection point during summer (from

190 November to the end of year) was identified as the EOS; and (iii) the POS was identified as the
191 date with the maximum EVI value during the growing season (Ma et al. 2013).

192 As for cropland, we assumed that the start of season (SOS), end of season (EOS) and peak of
193 season (POS) dates were the leaf emergence, crop harvest and crop heading dates observed from
194 remote sensing, respectively (Sakamoto et al. 2005). The length of the growing season (LOS) in
195 this paper was defined as the difference between the SOS and EOS. The growing season (GS)
196 was divided into the two stages of vegetation growth (VG) and reproductive growth (RG) by the
197 POS date.

198

199 2.3 Methodology

200 2.3.1 Variability indicator

201 Mathematically, in the time series profile of EVI, technological improvements in farming
202 practices (inter-annual trend), phenology (seasonality, the time of turning points in crop growth
203 and development), the vegetation variation caused by climate variability (inter-annual variation),
204 and the system observational errors are subject to trend, seasonal, anomaly and noise components
205 (Shumway & Stoffer 2010), respectively. Here, the noise component can be reduced by unifying
206 the temporal and spatial scale of EVI and LST. We assumed the technology in farming practices
207 was at an average level from 2001 to 2013 and adopted a standardized anomaly (Sa-s) to
208 represent the inter-annual variability of EVI, and similarly to each of the other variable.

$$209 \quad x'_{d,y} = (x_{d,y} - \bar{x}_d) / \bar{x}_d \quad (1)$$

210 $x_{d,y}$ is a single element of a time-series variable X ; x' is the anomaly value of each variable at
 211 the dth 8-day time point in the yth year; and \bar{x} is the mean value at the dth 8-day time
 212 point throughout the period from 2001 to 2013. The time series sequence of Sa-s excluded the
 213 seasonality of the original data sequence without collinearity with the other variables. The 8-day
 214 Sa-s values of Rain, T_{max} , T_{min} , Radn, LST and EVI for the 161 selected points during 2001- 2013
 215 were calculated.

216

217 2.3.2 Thermal time reference

218 Converting the time reference from normal calendar time to thermal time allows to make an
 219 average consideration of crops in similar phenological stages among different years, and to
 220 remove the effects of spatial heterogeneity (Duveiller, Baret, et al. 2013; Duveiller,
 221 López-Lozano, et al. 2013). The thermal time theory is based on the time taken of plant growth
 222 and development, depending on temperature (Atwell 1999). Therefore, thermal time (tt) over a
 223 particular time period from t_1 to t_2 can be expressed as cumulated heat units (in growing degree
 224 days) (Duveiller, Baret, et al. 2013; Duveiller, López-Lozano, et al. 2013; Franch et al. 2015;
 225 Skakun et al. 2017):

$$226 \quad tt = \sum_{i=t_1}^{t_2} \left[\frac{(T_{max,i} + T_{min,i})}{2} - T_{base} \right] \quad (2)$$

227 In this case, the minimum (T_{min}) and maximum (T_{max}) air temperature are based on a daily time
 228 step. The base (T_{base}) temperature for winter wheat was set to 0 °C, and the starting date t_1 was
 229 arbitrarily fixed to 1st January of each year from year 2001 to 2013. If the average daily air
 230 temperature of T_{max} and T_{min} is below T_{base} , it would be replaced by T_{base} , and no growing degree

231 days are accumulated. Thermal time of EVI profiles were then calculated for each year but
232 having irregularly sampled time series. To make them comparable, a regular sampling steps of
233 100 growing degree days were thereafter linearly interpolated (Duveiller, Baret, et al. 2013).

234

235 2.3.3 Relative importance approach

236 To elucidate the unique correlation between a single climate component Sa-s and EVI Sa-s
237 without interference from other variables, we applied the partial correlation method (Chevan &
238 Sutherland 1991) by controlling the variance of the other 4 climate components. The package
239 ‘relaimpo’ in R (Grömping 2006) was applied to calculate the ranks of the climate components
240 for each 8-day time segment in terms of their unique contribution to EVI variation. Their unique
241 contributions were then rescaled to sum to R^2 , the total proportion of EVI variance explained by
242 climate variability, as the relative contribution of the climate components. The individual and
243 accumulated relative contributions of the selected climate variable Sa-s to the EVI Sa-s in the
244 growing season both across study area and at each testing pixel were then calculated.

245 In this paper, data processing and statistical analysis were performed in the R computation
246 environment, and related packages were obtained from The Comprehensive R Archive Network
247 (<http://cran.r-project.org>).

248

249 3 RESULTS

250 3.1 Crop growth seasonality and variability across the NSW wheat belt from 2001 to 2013

251 3.1.1 Crop growth seasonality and variability

252 The average annual EVI curve shown in Figure 2a represents the seasonality of vegetation
253 growth across the cropland belt from 2001 to 2013 in NSW. The profile and magnitude of the
254 curve and EVI variations are important indicators of vegetation growth. From the average EVI
255 seasonality shown in Figure 2a, it is apparent that there is only one major growing season across
256 the study area from leaf emergence (start of season; SOS date) at Day of the Year (DoY) 156,
257 which has an EVI value of 0.206, to harvest (end of season; EOS date) at DoY326, which has an
258 EVI value of 0.177. The length of the growing season (LOS) was 170 days, with a maximum EVI
259 value (peak of season; POS) of 0.373 at DoY 246. This indicates that the lengths of vegetative
260 growth (VG) and reproductive growth (RG) were 90 and 80 days, respectively. The actual
261 growing season of winter wheat planted in eastern Australia (Bowden et al. 2008) matches this
262 EVI curve well. At the same time, Figure 2d shows that the 13 years average EVI profile in
263 thermal time reference, winter crop across the study area appear at 3000 °C degree days and end
264 of senescence at 5500 °C. All the single-year EVI growing season start and end within 500
265 degree days with our average fixed growing season. The only differences are the shape and
266 amplitude of the curves.

267 ## Figure 2 insert here##

268 As Figure 2b shows, the variation of EVI in the growing season was significantly larger than in
269 the non-growing season, especially during the reproductive growth period, with a Sd of 16.7% at
270 DoY 153 near EOS, 18.2% at DoY 249 near POS, and 19.3% at DoY 257, and the Sd was greater
271 than 20% for the consecutive 8-day time segments from DoY 265 to DoY 313.

272

273 3.1.2 The key 8-day time segment of the crop growth cycle

274 To decide which 8-day segment of EVI in the crop growing season had the strongest correlation
275 with annual yield, we used the Pearson correlation method to analyze the 8-day EVIs and
276 observed wheat grain yield (t ha^{-1}) in NSW at the 117 ground trial sites from 2005 to 2013 for
277 which observational data were available. The 8-day EVIs were positively correlated with the
278 wheat yield throughout the growing season, particularly during the reproductive growth stage
279 (Figure 2c). The correlation coefficient at the 8-day time segment, start from DoY 153,
280 immediately before leaf emergence was 0.16, and it increased to 0.47 after the heading date (POS)
281 at DoY 249. It increased significantly during the rest of RG and reached its peak at DoY 289,
282 with a value of 0.76. This indicates that the larger the EVI value at DoY 289, the higher the
283 annual yield, and *vice versa*.

284 The slope of EVI at each 8-day time segment from 2001 to 2013 fluctuated notably during the
285 growing season (Figure 2c). The slopes were positive during the vegetative growth (VG) phase,
286 but negative during the reproductive phase (RG). Thus, vegetation greenness increased during
287 VG, but decreased during RG. During RG, the trend value dropped by 0.001 each year following
288 POS and then dropped greatest by 0.003 each year at the 8-day time segment, from DoY 257.

289 As EVI at DoY257 also has a high correlation of 0.56 with annual yield, we identified the two
290 critical 8-day time segments, beginning from DoY257 and DoY 289, as the key 8-day ‘windows’
291 during the remotely sensed crop growth cycle.

292

293 3.2 Climate and LST seasonality and variability across the NSW wheat-belt in growing season

294 3.2.1 Climate and LST seasonality and variability

295 The overall annual climate and LST seasonality patterns (Table 1, Figure 3) across the NSW
296 wheat belt showed the typical characteristics of a temperate sub-humid climatic zone: warm in
297 the crop pre-growing season (pre-GS) and reproductive phase (RG) and cool in the crop
298 vegetative phase (VG), with moderate rainfall throughout the year. The average rainfall (Rain)
299 during the VG and RG was 114.1 and 99.5 mm, respectively, across the study area, and in pre-GS,
300 the average was 182.4, with a moderately even distribution throughout the crop growing season.
301 The ranges of the average daily T_{\max} , T_{\min} , Radn, and LST (canopy temperature) throughout the
302 GS were 30.1–15.3°C, 14.8–3.1°C, 25.9–9.2 MJ m⁻², and 39.4–13.7°C, respectively. The Sd
303 values of T_{\max} , LST and Radn in RG were mostly higher than those during the VG phase (Figure
304 3), while the variability of T_{\min} was larger at the beginning and end of the GS relative to the
305 middle stages of the GS. The variability of rain was irregular throughout the GS and peaked at
306 the 8-day time segment from DoY 289, with a Sd of 159%. The Sd provided in Table 1 shows the
307 overall climate and LST variability at a broader time-scale. All of the Sds in the RG phase were
308 much larger than those of the pre-GS and VG phases (Table 1). The variability of the climate and
309 LST in the VG was the lowest. LST showed the largest variability among all climate components,
310 especially during the RG (Table 1).

311 ## Figure 3 insert here##

312 ## Table 1 insert here##

313 During the 32nd 8-day period, near the heading date (DoY249), all of the heat factors, T_{\max} , T_{\min} ,
314 LST and Radn, showed an increasing trend from 2001 to 2013 (Figure 3), with slopes of 0.26°C
315 y⁻¹, 0.02°C y⁻¹, 0.11°C y⁻¹ and 0.12 MJ m⁻² y⁻¹, respectively. The EVI started to decrease at this
316 time point (Figure 2), with a decreasing rate of 0.001 y⁻¹. At the critical 8-day time segment from
317 DoY 257, T_{\min} and LST showed decreasing trends, with annual rates of 0.02°C y⁻¹ and 0.18°C y⁻¹.

318 Meanwhile, Radn and T_{\max} showed increasing trends, with annual rates of $0.14 \text{ MJ/m}^2/\text{yr}$ and
319 $0.18^\circ\text{C y}^{-1}$, respectively. At the other critical 8-day time segment from DoY 289, T_{\max} and T_{\min}
320 had the same trends as at the 8-day segment from DoY 257. However, LST had an increasing
321 trend, with a rate of $0.11^\circ\text{C y}^{-1}$, and Radn had a decreasing trend, with a rate of $0.01 \text{ MJ m}^{-2} \text{ y}^{-1}$.

322

323 3.2.2 Spatial variation of the 13-year average iEVI and climate conditions

324 The average annual iEVI across the NSW cropland belt ranged from 3.84 to 9.96 (Figure 4). The
325 iEVI in the southeastern part of the study area was almost twice as large compared with the upper
326 northern part, with an average value of 8.9 in the southeast and 4.8 in the upper north part of the
327 NSW wheat belt.

328 ## Figure 4 insert here##

329 Correspondence was observed for the spatial distribution of rainfall in the southern part, but not
330 in the northern part, of study area. The average annual rainfall during the GS ranged from 123.2
331 mm in the west to 320.6 mm in the east and displayed a typical E-W spatial gradient that was
332 distributed based on the pixels' distance to the coast. The growing season Radn, T_{\max} , LST and
333 T_{\min} followed a similar N-S temperature spatial gradient distribution pattern, which was higher in
334 the north and lower in the southeast. Their range differences were 3.5 MJ m^{-2} , 7.6°C , 11.5°C ,
335 5.9°C , respectively.

336

337 3.3 Contributions of climate and LST variability to crop growth variation over the GS

338 3.3.1 Individual impacts of climate and LST on EVI variation at a regional scale

361 3.3.2 Accumulated relative contributions of the climate variability to the EVI variability

362 Figure 6 shows the contributions of the inter-annual climate variation to variations in EVI at the
363 8-day time scale during the growing season (GS). The total effects of climate variation showed an
364 increasing trend throughout the GS and accounted for 83.3% at the 8-day time segment from
365 DoY 169 during the VG and 97.1% at the segment from DoY 289 during the RG on EVI Sa-s
366 across the NSW croplands belt. At the critical time segment from DoY 257, the total climatic
367 contribution increased from 47.6% from the previous 8-day time segment to 88.3%, while the
368 EVI value dropped sharply by 0.003 each year (Figure 2c).

369 ## Figure 6 insert here##

370 In the rainfed NSW cropland belt, the proportion of rain Sa-s to the total climate contributions
371 peaked at the 8-day time segment from DoY 169, which was the tillering stage of the vegetative
372 growth phase (VG), with a value of 50.6%, and then declined steadily throughout the VG and
373 increased moderately during the reproductive growth phase (RG). At the critical 8-day window
374 from DoY 257, it accounted for 21.8% of the variation in the EVI. The proportion of the LST
375 variation among the total climate contribution increased from the VG to the RG and accounted
376 for 65.8% at the critical 8-day window from DoY 289. It was more than half of the total climate
377 contribution at that time segment. During the RG, the LST was the single most important climate
378 factor that affected EVI variability in 9 out of 10 8-day time segments across the NSW cropland
379 belt.

380 T_{\min} explained a large proportion of the impact of climate variation on the change in EVI
381 immediately before peak of the season date (POS), the corresponding crop heading date. It
382 reached its peak at the 8-day time segment from DoY 233, with a value of 46.5%. The

383 contribution of T_{\max} variation to the EVI Sa-s was larger during the RG than the VG, but more
384 moderate than the LST Sa-s. It peaked at the 8-day time segment from DoY 265, with a value of
385 37.3%. Radn Sa-s affected the EVI Sa-s steadily from approximately 10% to 20% throughout the
386 GS across the study area.

387

388 3.3.3 Spatial distribution of the climate and LST variability contributions to EVI variation

389 The individual and accumulated contributions of climate and LST Sa-s to EVI Sa-s at every
390 selected pixel during the GS were demonstrated in Figure 7. The inter-annual total climate
391 variability at the 8-day time scale caused EVI variations from 5.94% to 42.09% across the study
392 area from 2001–2013. The total effects were higher in the north and southwestern parts of the
393 NSW wheat belt relative to the middle parts.

394 *## Figure 7 insert here##*

395 Variation in LST was the most important climate factor influencing variation in EVI. The
396 contribution ranged from 3.24% to 34.47% across the cropland belt in NSW. The spatial
397 distribution was largest in the northern and southwestern parts of the study area. The relative
398 importance of the total variability of total rain was smaller, with a maximum contribution of
399 3.57% to EVI variation, and its importance was larger in the western and middle parts of the
400 NSW wheat belt. The importance of variation in Radn that caused variability in EVI was largest
401 on the eastern parts of the cropland belt, with a range from 0.2% to 3.27%. The contribution
402 range of T_{\max} was 0.28% to 10.27%, with a gradual trend from east to west. The effects of T_{\min}
403 Sa-s ranged from 0.08% to 4.08% for EVI Sa-s across the study area, and they were greater in the
404 relatively cooler areas of the southeastern and middle parts of the study area.

405

406 4 DISCUSSION

407 4.1 Ability of the MODIS EVI profile to represent rainfed cropland productivity in Australia

408 The start and end dates of the growth season (SOS and EOS) of winter crops are relatively fixed
409 compared to the considerable variability observed in native grasses and shrubs (Bowden et al.
410 2008). SOS and EOS are not merely determined by climate because human management and
411 farmers' experience can largely control them. Although there is sowing date guidance offered
412 based on rainfall (Keating et al. 2002), farmers still sow even if rainfall does not reach the
413 required levels during June to avoid heat stress in the following summer. Variations in the timing
414 of the different growth stages are thereafter largely affected by climate variability, especially in
415 broadacre rainfed cropping systems. The EVI profile in thermal time reference has shown the
416 relatively fixed growing season across the NSW wheat belt, we could measure the relative
417 contributions of climate variation to crop growth variability at every 8-day time segment.

418 The MODIS EVI-fitted GS in this study starts at DoY 156 in early June ends at DoY 326 in late
419 November, with a length of 170 days. The average peak of season (POS) date occurs at DoY 246
420 in September, with an EVI value of 0.373. This phenology matches well with the observed wheat
421 life cycle in eastern Australia (Bowden et al. 2008). Based on observations of 117 trials, the
422 average sowing and harvest dates across the NSW wheat belt are DoY 145 (± 1.5 days) and DoY
423 326 (± 1.2 days), respectively. There could be an allowance of 11 days for seeds to establish from
424 the sowing date to the leaf emergence date (SOS, DoY156). The average harvest date had the
425 same date with the MODIS EVI derived end of season (EOS) date, DoY 326. Meanwhile, the
426 iEVI was significantly and linearly correlated with the *in-situ* grain yield among the trials each

427 year as well as among all sites (Figure 8). The overall R^2 was 0.755, while the relationship best
428 fit the 11 trials in year 2009, with an R^2 of 0.940. These results not only indicate that wheat is the
429 largest major winter crop planted across the NSW cropland but also indicate that the MODIS EVI
430 is capable of monitoring the winter wheat growth cycle in broadacre rainfed cropping systems.

431 `## Figure 8 insert here##`

432 The ability of the MODIS EVI to capture information related to crop growth and development
433 has also been tested (Bolton & Friedl 2013) in the central United States. The authors concluded
434 that MODIS products have good potential applications for agricultural monitoring in areas with
435 large field sizes, as is the case in Australian wheat cropping in NSW. The MODIS-derived
436 average annual time-series profile of the EVI (Figure 2a) reflects the actual crop growth
437 conditions across the NSW wheat belt. Over the entire crop life span, the correlation coefficient
438 between EVIs and the actual yield peaks at the 8-day time segment from DoY 289, with a value
439 of 0.76 (Figure 2c). Thus, the stability and range of EVI values at this critical time segment had
440 the highest direct correlation and ensured an annual attainable yield.

441

442 4.2 Impacts of climate and LST variability on the variation of the EVI in key crop growth stages

443 The trend of EVI values at every 8-day segment can be explained not only by the
444 delayed/advance of the growing season but also by the technological improvement that modifies
445 wheat crop traits as well as the interference of weather extremes on crop radiometric reflection.
446 From 2001 to 2013, farmers improved the biomass of wheat crops during vegetative growth
447 phase (VG) across the NSW cropland belt, but neglected the importance of plant biomass
448 accumulation during the reproductive growth phase (RG) (Figure 2c). The sharpest drop of EVI

449 at the 8-day time segment from DoY 257 made it the most sensitive to climate variability during
450 this period.

451 The relative importance of the proportion of rain, T_{\max} , T_{\min} , Radn and LST Sa-s to EVI Sa-s
452 reached its peak at the 8-day time segments from DoY 169 (VG), DoY 265 (RG), DoY 233 (VG),
453 DoY 217 (VG), and DoY 289 (RG), respectively (Figure 6), across the NSW wheat belt during
454 2001-2013. In the semi-arid rain-fed environment, the lack of rainfall and resultant water stress is
455 inevitably one of the most serious climatic limiting factors to crop establishment and
456 development (Asseng et al. 2011), especially around the tilling stage (the 8-day time segment
457 from DoY 169, where Rain is the most important climate factor) during VG. However, during
458 RG, heat stress is more evident because temperature has a relatively higher base during this phase,
459 which is sometimes higher than the optimum wheat growth air temperature of 23°C
460 (www.agric.wa.gov.au). The cropland maximum air temperature and canopy temperature
461 reached >30°C during the RG (Figure 3) across the study area. In particular, fluctuations of
462 T_{\max} and LST during a sensitive stage of crop development, such as the grain growth stage (the
463 8-day time segment from DoY289), can significantly reduce grain yield due to their direct effects
464 on leaf photosynthesis, grain number and grain mass (Talukder et al. 2014), while a continuous
465 period of extremely high temperatures can result in physiological damage and almost total yield
466 loss (Asseng et al. 2011; Lobell et al. 2012). At the critical 8-day segments from DoY 257 and
467 289, identified in this study (part 3.1.2), which corresponded to the wheat flowering and grain
468 growth stages, respectively, the impacts of heat variation outweighed the impact of variation in
469 rainfall on EVI by more than twofold.

470 During RG, variation of LST was the most important factor that contributed to variation of EVI.
471 LST, the canopy temperature, quantifies the combined indirect effects of air temperature,

472 radiation and effective rainfall within the soil-plant-atmosphere continuum. A higher LST reflects
473 lower latent heat flux from the canopy, which indicates lower canopy evapotranspiration and
474 higher heat stress conditions (Li et al. 2010). The remotely sensed estimation of surface
475 temperature has proven to be a well suited ground canopy temperature indicator in large-scale
476 crop monitoring (Karnieli et al. 2010; Sandholt et al. 2002). It simultaneously measures the
477 comprehensive water and heat stress conditions caused by interactions among climatic driving
478 factors. Thus, the impacts of the LST variation on the variation of the EVI increased in the hotter
479 northern and drier southwestern parts of the NSW wheat belt.

480

481 5 CONCLUSIONS

482 In this study, we quantified the spatio-temporal impacts of variation in climate and land surface
483 temperature (LST) on the variation of crop EVI at key crop growth stages. The standard anomaly
484 method was adopted to indicate the variability of all variables at an 8-day time scale. We found
485 that a single major crop growing season (GS), occurred in the second half of the year across the
486 NSW wheat belt during 2001–2013. Two critical 8-day time segments, beginning from DoY 257
487 and 289, were identified as the key ‘windows’ during the winter crop GS, that is, the variation in
488 climate during these 8-day time segments exerted a greater impact on the grain yield than during
489 any other periods during the GS.

490 Our results show that the total climate variation during the two 8-day ‘windows’ contributed
491 more than 88% of the variability in EVI, of which the LST accounted for more than half.
492 Therefore, more attention should be paid to the LST during implementation of large-scale rainfed
493 cropland monitoring. As such, once an association model (i.e. linear regression model) among

494 LST, EVI and annual grain yield is built-up (Kumar 1998), we could estimate and predict grain
495 yield during these two key 8-day “windows” (approximately one month) before the crop is
496 harvested. Spatially, the total contribution of climate variation during the GS accounted for up to
497 42% of the variability in the EVI, especially in the northern and southwestern regions of the
498 NSW wheat belt. As an index that integrates the indirect effects of the complex interactions
499 among all the climate-driving factors on crop growth, the LST is the first dominant climate
500 component that affects the variability of the EVI across those regions.

501 The limitation of this study was the limited years (13 years) of data, which could cause
502 over-fitted models in the analysis. Because the time period from 2001-2013 was the period that
503 saw a shift from extreme drought to flood at a surprising speed (Dijk et al. 2013), the shift was
504 typically significant. We thereafter targeted this specific period of time and evaluated the
505 relationship between climate and crop growth in variability. This study also narrowed the analyze
506 time slot from annual to 8-days, which is the attainable temporal scale by MODIS EVI and LST,
507 to make it possible investigating the diverse crop-climate relationship over the crop life span.
508 However, in consideration of the comparison of the model performance among this time period
509 (2001-2013) and other years before and after, we will adopt additional datasets to expand the
510 number of sample years and build the best fit model in the future.

511

512 ACKNOWLEDGEMENTS

513 The Authors wish to thank Dr. Hao Shi, and Dr. Zunyi Xie for their helpful suggestions with this
514 study. We are grateful to Grains Research and Development Corporation (GRDC) National
515 Variety Trials (NVT), Australia (<http://www.nvtonline.com.au/>) for their data support. The first

516 author acknowledges the financial support from Chinese Scholarship Council, Ministry of
517 Education, China, as well as Dr. Sabina Belli and Mrs Ann-Maree Dombroski for their
518 suggestions on the grammar of this paper.

519

521 REFERENCES

- 522 Anwar, M.R., O’Leary, G., McNeil, D., Hossain, H. & Nelson, R. 2007, 'Climate change impact on rainfed
523 wheat in south-eastern Australia', *Field Crops Research*, vol. 104, no. 1–3, pp. 139-47.
- 524 Asseng, S., Foster, I.A.N. & Turner, N.C. 2011, 'The impact of temperature variability on wheat yields',
525 *Global Change Biology*, vol. 17, no. 2, pp. 997-1012.
- 526 Atwell, B.J. 1999, *Plants in action: adaptation in nature, performance in cultivation*, Macmillan Education
527 AU.
- 528 Barlow, K.M., Christy, B.P., O’Leary, G.J., Riffkin, P.A. & Nuttall, J.G. 2015, 'Simulating the impact of
529 extreme heat and frost events on wheat crop production: A review', *Field Crops Research*, vol.
530 171, pp. 109-19.
- 531 Biradar, C.M., Thenkabail, P.S., Noojipady, P., Li, Y., Dheeravath, V., Turrall, H., Velpuri, M., Gumma, M.K.,
532 Gangalakunta, O.R.P., Cai, X.L., Xiao, X., Schull, M.A., Alankara, R.D., Gunasinghe, S. & Mohideen,
533 S. 2009, 'A global map of rainfed cropland areas (GMRCA) at the end of last millennium using
534 remote sensing', *International Journal of Applied Earth Observation and Geoinformation*, vol. 11,
535 no. 2, pp. 114-29.
- 536 Bolton, D.K. & Friedl, M.A. 2013, 'Forecasting crop yield using remotely sensed vegetation indices and
537 crop phenology metrics', *Agricultural and Forest Meteorology*, vol. 173, pp. 74-84.
- 538 Bowden, P., Edwards, J., Ferguson, N., Nee, T.M., Manning, B., Roberts, K., Schipp, A., Schulze, K. &
539 Wilkins, J. 2008, *Wheat growth and development*, NSW Department of Primary Industries.
- 540 Broich, M., Huete, A., Paget, M., Ma, X., Tulbure, M., Coupe, N.R., Evans, B., Beringer, J., Devadas, R. &
541 Davies, K. 2015, 'A spatially explicit land surface phenology data product for science, monitoring
542 and natural resources management applications', *Environmental Modelling & Software*, vol. 64,
543 pp. 191-204.
- 544 Calzadilla, A., Rehdanz, K., Betts, R., Falloon, P., Wiltshire, A. & Tol, R.J. 2013, 'Climate change impacts on
545 global agriculture', *Climatic Change*, vol. 120, no. 1-2, pp. 357-74.
- 546 Chevan, A. & Sutherland, M. 1991, 'Hierarchical Partitioning', *The American Statistician*, vol. 45, no. 2, pp.
547 90-6.
- 548 Cleverly, J., Eamus, D., Luo, Q., Restrepo Coupe, N., Kljun, N., Ma, X., Ewenz, C., Li, L., Yu, Q. & Huete, A.
549 2016, 'The importance of interacting climate modes on Australia’s contribution to global carbon
550 cycle extremes', *Scientific Reports*, vol. 6, p. 23113.
- 551 Cohn, A.S., VanWey, L.K., Spera, S.A. & Mustard, J.F. 2016, 'Cropping frequency and area response to
552 climate variability can exceed yield response', *Nature Clim. Change*, vol. advance online
553 publication.
- 554 Cong, N., Wang, T., Nan, H., Ma, Y., Wang, X., Myneni, R.B. & Piao, S. 2013, 'Changes in satellite-derived
555 spring vegetation green-up date and its linkage to climate in China from 1982 to 2010: a
556 multimethod analysis', *Global Change Biology*, vol. 19, no. 3, pp. 881-91.
- 557 Dijk, A.I., Beck, H.E., Crosbie, R.S., Jeu, R.A., Liu, Y.Y., Podger, G.M., Timbal, B. & Viney, N.R. 2013, 'The
558 Millennium Drought in southeast Australia (2001–2009): Natural and human causes and
559 implications for water resources, ecosystems, economy, and society', *Water Resources Research*,
560 vol. 49, no. 2, pp. 1040-57.
- 561 Duveiller, G., Baret, F. & Defourny, P. 2013, 'Using thermal time and pixel purity for enhancing
562 biophysical variable time series: an interproduct comparison', *IEEE Transactions on Geoscience
563 and Remote Sensing*, vol. 51, no. 4, pp. 2119-27.

564 Duveiller, G., López-Lozano, R. & Baruth, B. 2013, 'Enhanced Processing of 1-km Spatial Resolution fAPAR
565 Time Series for Sugarcane Yield Forecasting and Monitoring', *Remote Sensing*, vol. 5, no. 3, p.
566 1091.

567 Eamus, D., Huete, A. & Yu, Q. 2016, *Vegetation Dynamics: A Synthesis of Plant Ecophysiology, Remote*
568 *Sensing and Modelling*, Cambridge University Press, 43-341.

569 Field, C.B., Barros, V.R., Mach, K. & Mastrandrea, M. 2014, 'Climate change 2014: impacts, adaptation,
570 and vulnerability', *Contribution of Working Group II to the Fifth Assessment Report of the*
571 *Intergovernmental Panel on Climate Change*.

572 Franch, B., Vermote, E.F., Becker-Reshef, I., Claverie, M., Huang, J., Zhang, J., Justice, C. & Sobrino, J.A.
573 2015, 'Improving the timeliness of winter wheat production forecast in the United States of
574 America, Ukraine and China using MODIS data and NCAR Growing Degree Day information',
575 *Remote Sensing of Environment*, vol. 161, no. Supplement C, pp. 131-48.

576 Godfray, H.C.J., Beddington, J.R., Crute, I.R., Haddad, L., Lawrence, D., Muir, J.F., Pretty, J., Robinson, S.,
577 Thomas, S.M. & Toulmin, C. 2010, 'Food security: the challenge of feeding 9 billion people',
578 *science*, vol. 327, no. 5967, pp. 812-8.

579 Gong, Z., Kawamura, K., Ishikawa, N., Goto, M., Wulan, T., Alateng, D., Yin, T. & Ito, Y. 2015, 'MODIS
580 normalized difference vegetation index (NDVI) and vegetation phenology dynamics in the Inner
581 Mongolia grassland', *Solid Earth*, vol. 6, pp. 1185-94.

582 Grömping, U. 2006, 'Relative Importance for Linear Regression in R: The Package relaimpo', *Journal of*
583 *Statistical Software*, vol. 17, no. 1, pp. 1-27.

584 Guo, L., An, N. & Wang, K. 2016, 'Reconciling the discrepancy in ground- and satellite-observed trends in
585 the spring phenology of winter wheat in China from 1993 to 2008', *Journal of Geophysical*
586 *Research: Atmospheres*, vol. 121, no. 3, pp. 1027-42.

587 Hamblin, A. 2009, 'Policy directions for agricultural land use in Australia and other post-industrial
588 economies', *Land Use Policy*, vol. 26, no. 4, pp. 1195-204.

589 Hochman, Z., Gobbett, D.L. & Horan, H. 2017, 'Climate trends account for stalled wheat yields in
590 Australia since 1990', *Global Change Biology*, vol. 23, pp. 2071-81.

591 Karnieli, A., Agam, N., Pinker, R.T., Anderson, M., Imhoff, M.L., Gutman, G.G., Panov, N. & Goldberg, A.
592 2010, 'Use of NDVI and Land Surface Temperature for Drought Assessment: Merits and
593 Limitations', *Journal of Climate*, vol. 23, no. 3, pp. 618-33.

594 Keating, B.A., Gaydon, D., Huth, N.I., Probert, M.E., Verburg, K., Smith, C.J. & Bond, W. 2002, 'Use of
595 modelling to explore the water balance of dryland farming systems in the Murray-Darling Basin,
596 Australia', *European Journal of Agronomy*, vol. 18, no. 1-2, pp. 159-69.

597 Kumar, V. 1998, 'An early warning system for agricultural drought in an arid region using limited data',
598 *Journal of Arid Environments*, vol. 40, no. 2, pp. 199-209.

599 Lawrence, G., Richards, C. & Lyons, K. 2013, 'Food security in Australia in an era of neoliberalism,
600 productivism and climate change', *Journal of Rural Studies*, vol. 29, no. 0, pp. 30-9.

601 Li, L., Nielsen, D.C., Yu, Q., Ma, L. & Ahuja, L.R. 2010, 'Evaluating the Crop Water Stress Index and its
602 correlation with latent heat and CO₂ fluxes over winter wheat and maize in the North China
603 plain', *Agricultural Water Management*, vol. 97, no. 8, pp. 1146-55.

604 Li, Z.-L., Tang, B.-H., Wu, H., Ren, H., Yan, G., Wan, Z., Trigo, I.F. & Sobrino, J.A. 2013, 'Satellite-derived
605 land surface temperature: Current status and perspectives', *Remote Sensing of Environment*, vol.
606 131, pp. 14-37.

607 Lobell, D.B., Sibley, A. & Ivan Ortiz-Monasterio, J. 2012, 'Extreme heat effects on wheat senescence in
608 India', *Nature Clim. Change*, vol. 2, no. 3, pp. 186-9.

609 Lymburner, L., Tan, P., Mueller, N., Thackway, R., Lewis, A., Thankappan, M., Randall, L., Islam, A. &
610 Senarath, U. 2010, '250 metre dynamic land cover dataset of Australia', *Geoscience Australia,*
611 *Canberra*.

612 Ma, X., Huete, A., Cleverly, J., Eamus, D., Chevallier, F., Joiner, J., Poulter, B., Zhang, Y., Guanter, L., Meyer,
613 W., Xie, Z. & Ponce-Campos, G. 2016, 'Drought rapidly diminishes the large net CO₂ uptake in
614 2011 over semi-arid Australia', *Scientific Reports*, vol. 6, p. 37747.

615 Ma, X., Huete, A., Moran, S., Ponce-Campos, G. & Eamus, D. 2015, 'Abrupt shifts in phenology and
616 vegetation productivity under climate extremes', *Journal of Geophysical Research:
617 Biogeosciences*, pp. 2036-52.

618 Ma, X., Huete, A., Yu, Q., Coupe, N.R., Davies, K., Broich, M., Ratana, P., Beringer, J., Hutley, L.B. &
619 Cleverly, J. 2013, 'Spatial patterns and temporal dynamics in savanna vegetation phenology
620 across the North Australian Tropical Transect', *Remote sensing of Environment*, vol. 139, pp.
621 97-115.

622 Ma, Y., Wang, S., Zhang, L., Hou, Y., Zhuang, L., He, Y. & Wang, F. 2008, 'Monitoring winter wheat growth
623 in North China by combining a crop model and remote sensing data', *International Journal of
624 Applied Earth Observation and Geoinformation*, vol. 10, no. 4, pp. 426-37.

625 Moulin, S., Bondeau, A. & Delecalle, R. 1998, 'Combining agricultural crop models and satellite
626 observations: From field to regional scales', *International Journal of Remote Sensing*, vol. 19, no.
627 6, pp. 1021-36.

628 Piao, S., Fang, J., Zhou, L., Philippe, C. & Zhu, B. 2006, 'Variations in satellite-derived phenology in China's
629 temperate vegetation', *Global Change Biology*, vol. 12, no. 4, pp. 672-85.

630 Plant, R.E. 2012, *Spatial data analysis in ecology and agriculture using R*, cRc Press Boca Raton, Florida.

631 Ponce Campos, G.E., Moran, M.S., Huete, A., Zhang, Y., Bresloff, C., Huxman, T.E., Eamus, D., Bosch, D.D.,
632 Buda, A.R., Gunter, S.A., Scalley, T.H., Kitchen, S.G., McClaran, M.P., McNab, W.H., Montoya, D.S.,
633 Morgan, J.A., Peters, D.P.C., Sadler, E.J., Seyfried, M.S. & Starks, P.J. 2013, 'Ecosystem resilience
634 despite large-scale altered hydroclimatic conditions', *Nature*, vol. 494, no. 7437, pp. 349-52.

635 Potgieter, A., Apan, A., Hammer, G. & Dunn, P. 2011, 'Estimating winter crop area across seasons and
636 regions using time-sequential MODIS imagery', *International journal of remote sensing*, vol. 32,
637 no. 15, pp. 4281-310.

638 Rabbinge, R. 2007, 'The Ecological Background of Food Production', *Ciba Foundation Symposium 177 -
639 Crop Protection and Sustainable Agriculture*, John Wiley & Sons, Ltd., pp. 2-29.

640 Ray, D.K., Gerber, J.S., MacDonald, G.K. & West, P.C. 2015, 'Climate variation explains a third of global
641 crop yield variability', *Nature Communications*, vol. 6.

642 Reed, B.C., Brown, J.F., VanderZee, D., Loveland, T.R., Merchant, J.W. & Ohlen, D.O. 1994, 'Measuring
643 phenological variability from satellite imagery', *Journal of vegetation science*, vol. 5, no. 5, pp.
644 703-14.

645 Rosenzweig, C., Jones, J., Hatfield, J., Ruane, A., Boote, K., Thorburn, P., Antle, J., Nelson, G., Porter, C. &
646 Janssen, S. 2013, 'The agricultural model intercomparison and improvement project (AgMIP):
647 protocols and pilot studies', *Agricultural and Forest Meteorology*, vol. 170, pp. 166-82.

648 Sakamoto, T., Gitelson, A.A. & Arkebauer, T.J. 2013, 'MODIS-based corn grain yield estimation model
649 incorporating crop phenology information', *Remote Sensing of Environment*, vol. 131, no. 0, pp.
650 215-31.

651 Sakamoto, T., Yokozawa, M., Toritani, H., Shibayama, M., Ishitsuka, N. & Ohno, H. 2005, 'A crop
652 phenology detection method using time-series MODIS data', *Remote Sensing of Environment*, vol.
653 96, no. 3-4, pp. 366-74.

654 Sandholt, I., Rasmussen, K. & Andersen, J. 2002, 'A simple interpretation of the surface
655 temperature/vegetation index space for assessment of surface moisture status', *Remote Sensing
656 of Environment*, vol. 79, no. 2-3, pp. 213-24.

657 Shumway, R.H. & Stoffer, D.S. 2010, *Time series analysis and its applications: with R examples*, Springer
658 Science & Business Media.

- 659 Skakun, S., Franch, B., Vermote, E., Roger, J.-C., Becker-Reshef, I., Justice, C. & Kussul, N. 2017, 'Early
660 season large-area winter crop mapping using MODIS NDVI data, growing degree days
661 information and a Gaussian mixture model', *Remote Sensing of Environment*, vol. 195, no.
662 Supplement C, pp. 244-58.
- 663 Stokes, C. & Howden, M. 2010, *Adapting agriculture to climate change: preparing Australian agriculture,
664 forestry and fisheries for the future*, CSIRO PUBLISHING.
- 665 Talukder, A.S.M.H.M., McDonald, G.K. & Gill, G.S. 2014, 'Effect of short-term heat stress prior to
666 flowering and early grain set on the grain yield of wheat', *Field Crops Research*, vol. 160, pp.
667 54-63.
- 668 Tripathi, A., Tripathi, D.K., Chauhan, D.K., Kumar, N. & Singh, G.S. 2016, 'Paradigms of climate change
669 impacts on some major food sources of the world: A review on current knowledge and future
670 prospects', *Agriculture, Ecosystems & Environment*, vol. 216, pp. 356-73.
- 671 Wang, B., Chen, C., Liu, D.L., Asseng, S., Yu, Q. & Yang, X. 2015, 'Effects of climate trends and variability
672 on wheat yield variability in eastern Australia', *Climate Research*, vol. 64, no. 2, p. 173.
- 673 Wang, B., Liu, D.L., Asseng, S., Macadam, I. & Yu, Q. 2015, 'Impact of climate change on wheat flowering
674 time in eastern Australia', *Agricultural and Forest Meteorology*, vol. 209–210, pp. 11-21.
- 675 Wardlow, B.D. & Egbert, S.L. 2008, 'Large-area crop mapping using time-series MODIS 250 m NDVI data:
676 An assessment for the U.S. Central Great Plains', *Remote Sensing of Environment*, vol. 112, no. 3,
677 pp. 1096-116.
- 678 Xie, Z., Huete, A., Restrepo-Coupe, N., Ma, X., Devadas, R. & Caprarelli, G. 2016, 'Spatial partitioning and
679 temporal evolution of Australia's total water storage under extreme hydroclimatic impacts',
680 *Remote Sensing of Environment*, vol. 183, pp. 43-52.
- 681 Yu, Q., Hengsdijk, H. & Liu, J.D. 2001, 'Application of a progressive-difference method to identify climatic
682 factors causing variation in the rice yield in the Yangtze Delta, China', *International Journal of
683 Biometeorology*, vol. 45, no. 2, pp. 53-8.
- 684 Yu, Q., Li, L., Luo, Q., Eamus, D., Xu, S., Chen, C., Wang, E., Liu, J. & Nielsen, D.C. 2014, 'Year patterns of
685 climate impact on wheat yields', *International Journal of Climatology*, vol. 34, no. 2, pp. 518-28.
- 686 Zheng, B., Chenu, K., Fernanda Dreccer, M. & Chapman, S.C. 2012, 'Breeding for the future: what are the
687 potential impacts of future frost and heat events on sowing and flowering time requirements for
688 Australian bread wheat (*Triticum aestivum*) varieties?', *Global Change Biology*, vol. 18, no. 9, pp.
689 2899-914.

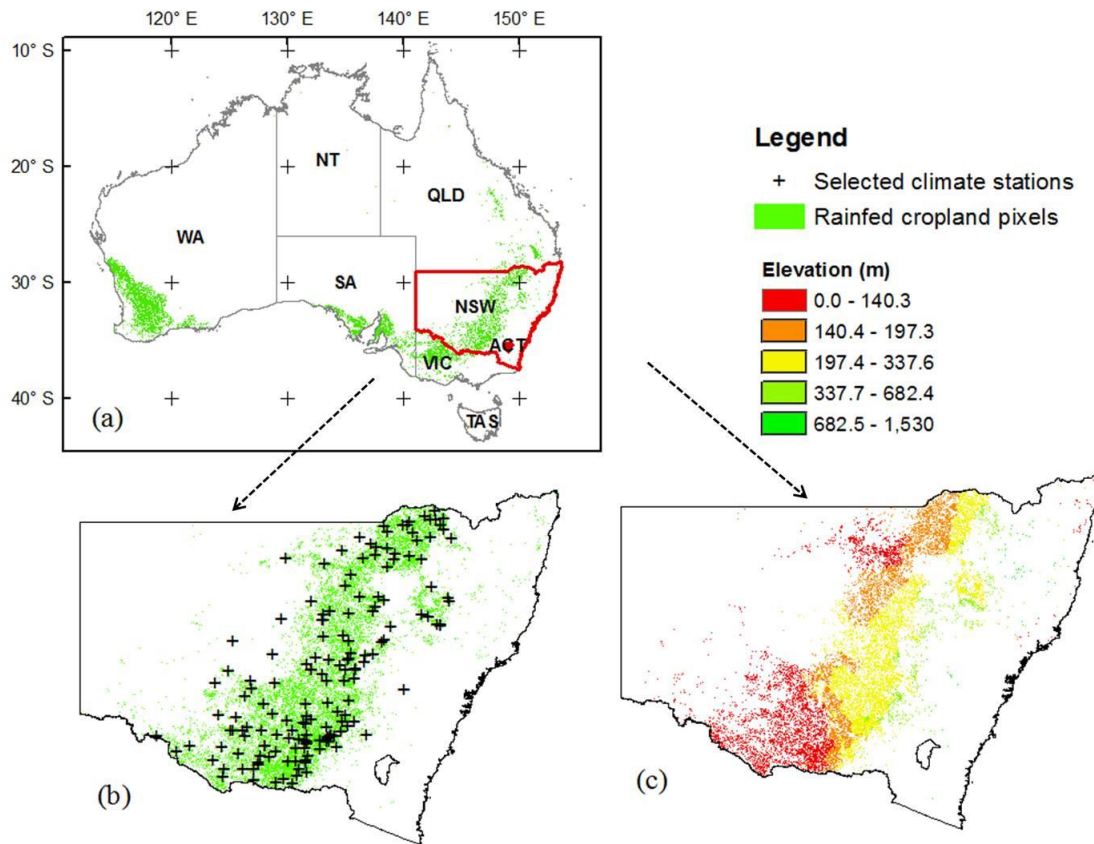
690

691

692 FIGURES

693

694



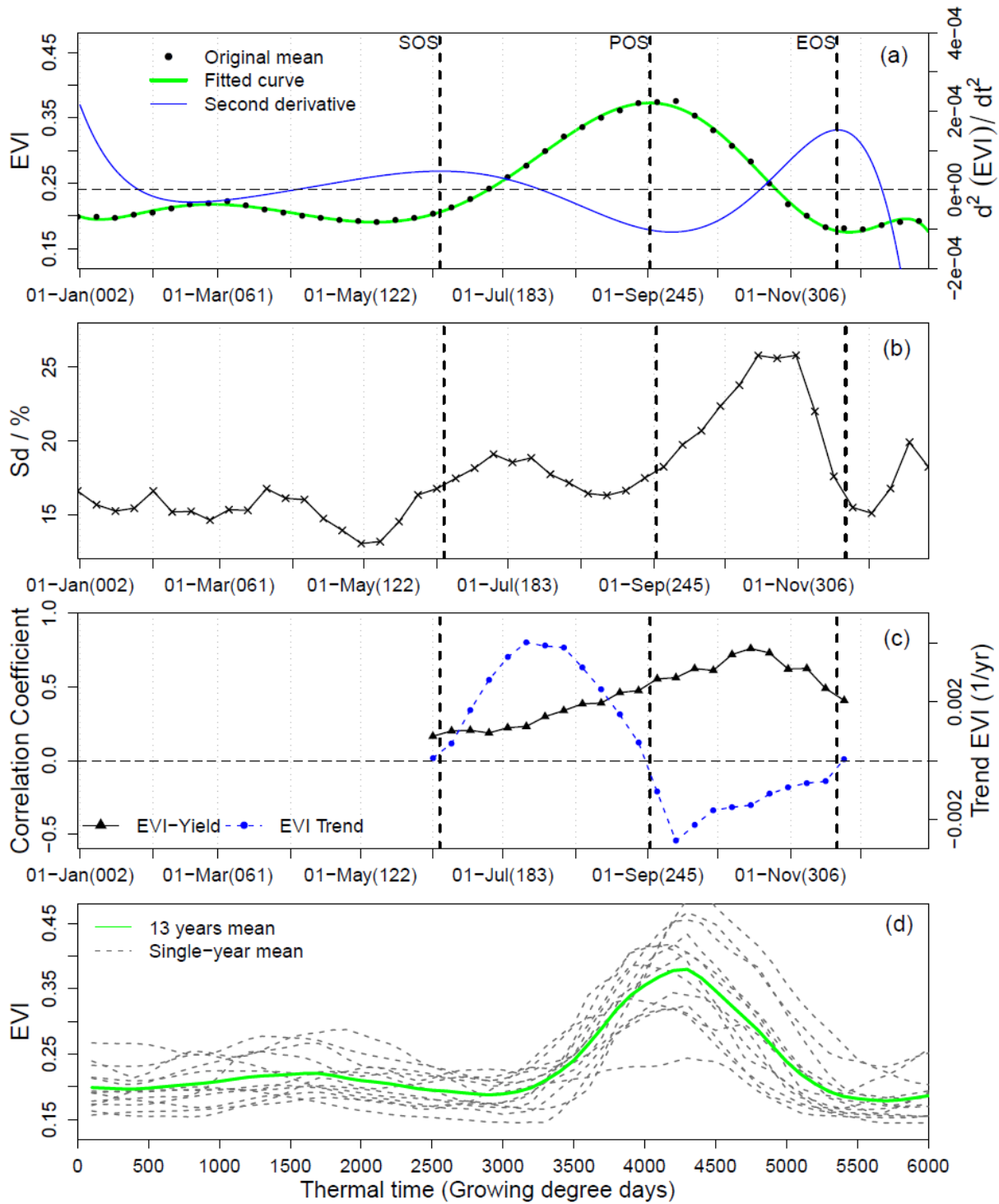
695

696 **Figure 1** Spatial distribution of the NSW rainfed cropland belt and locations of selected testing

697 pixels. The green areas are the gridded rainfed cropland belts across Australia (a) and NSW (b); (c)

698 elevation map of the NSW rainfed cropland belt

699



700

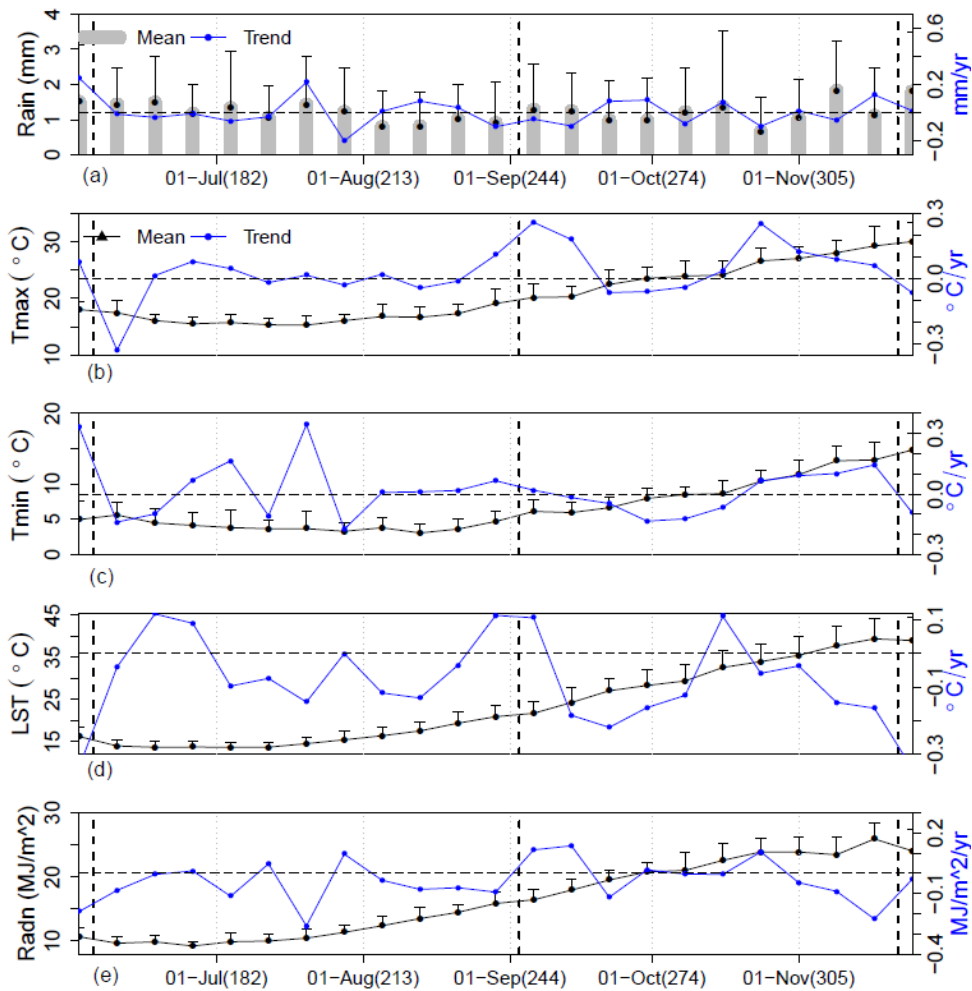
701 **Figure 2** Variation and trend of the average seasonal EVI profile in the NSW rainfed cropland belt

702 from 2001 to 2013 and correlations of the 8-day EVIs with observed annual grain yield. (a) Black

703 dots: average EVI values for all of the testing points from 2001 to 2013; green solid line: fitted EVI

704 curve; blue solid line: second derivative; POS: peak of season (heading date); SOS: start of season
 705 (leaf emergence date); EOS: end of season (harvest date). (b) One standard deviation (Sd in %) of
 706 the 13-year period. (c) Blue dashed line with circle solid dots: EVI trends at each 8-day time point
 707 from 2001 to 2013. Black solid line with triangular solid dots: correlations between the 8-day EVIs
 708 and annual grain yield at 117 trial sites. X-axis of (a) to (c): Date (Day of the Year). (d) green solid
 709 line: 13 years mean EVI in the time reference of thermal time (growing degree days, °C). grey
 710 dashed lines: single-year means of EVI from 2001 to 2013.

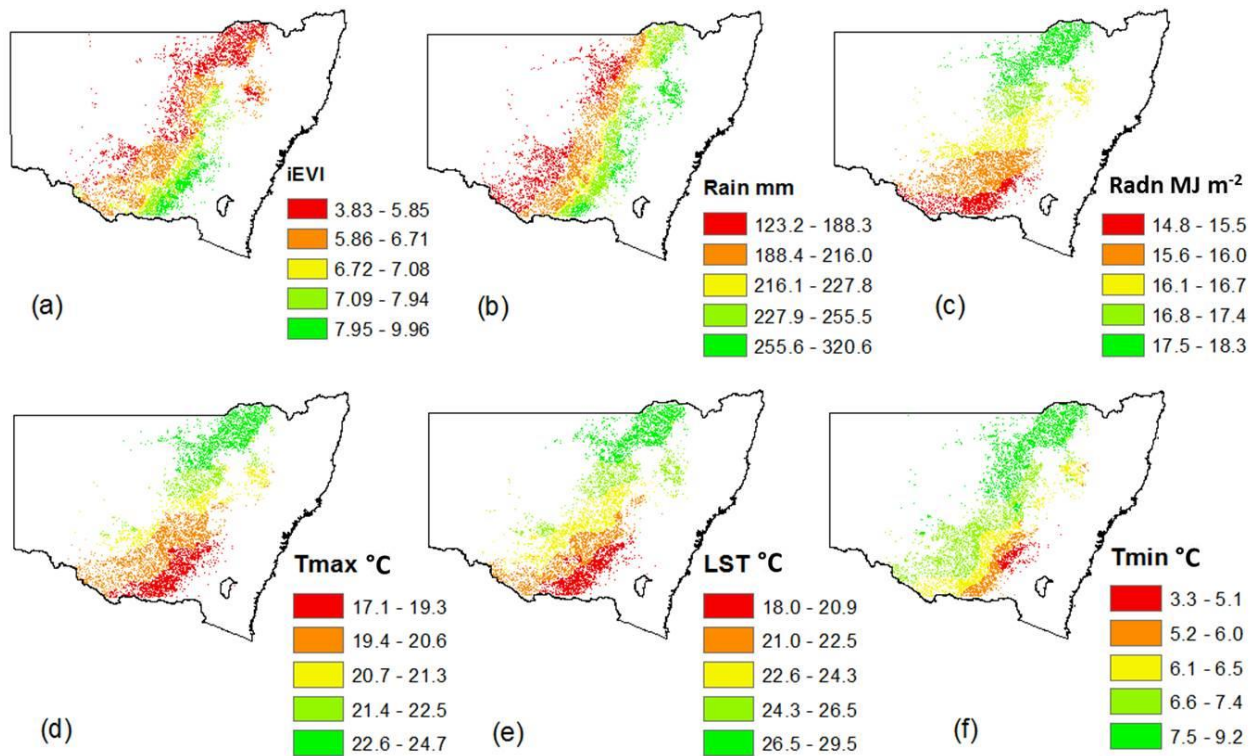
711



712

713 **Figure 3** Growing season climate and LST seasonality as well as their variability and trend at
 714 each 8-day time segment from 2001 to 2013 across the NSW cropland belt. (a) Rainfall; (b)
 715 maximum air temperature; (c) minimum air temperature; (d) land surface temperature; (e) solar
 716 radiation. Black solid curves: seasonality (primary y-axis). Error bars: one standard deviation
 717 (Sd). Blue solid curves: trends at each 8-day time segment over 13 years (second y-axis). Black
 718 horizontal dash line: 0 line (second y-axis). X-axis: Date (Day of Year)

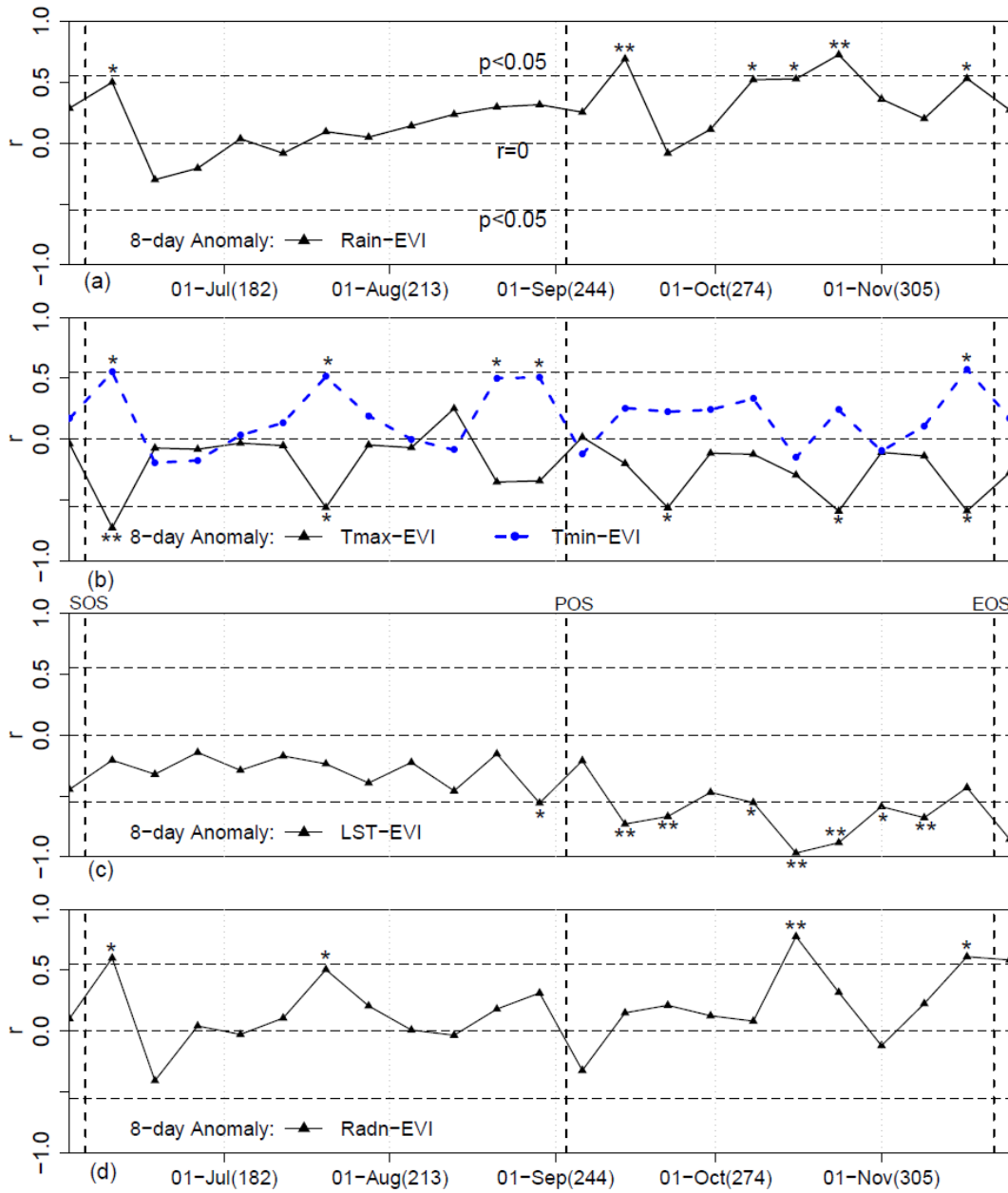
719



720

721 **Figure 4** Spatial variations of the 13-year average iEVI as well as growing season climate and LST
 722 conditions. (a) iEVI; (b) rainfall; (c) radiation; (d) maximum air temperature; (e) land surface
 723 temperature; (f) minimum air temperature

724



725

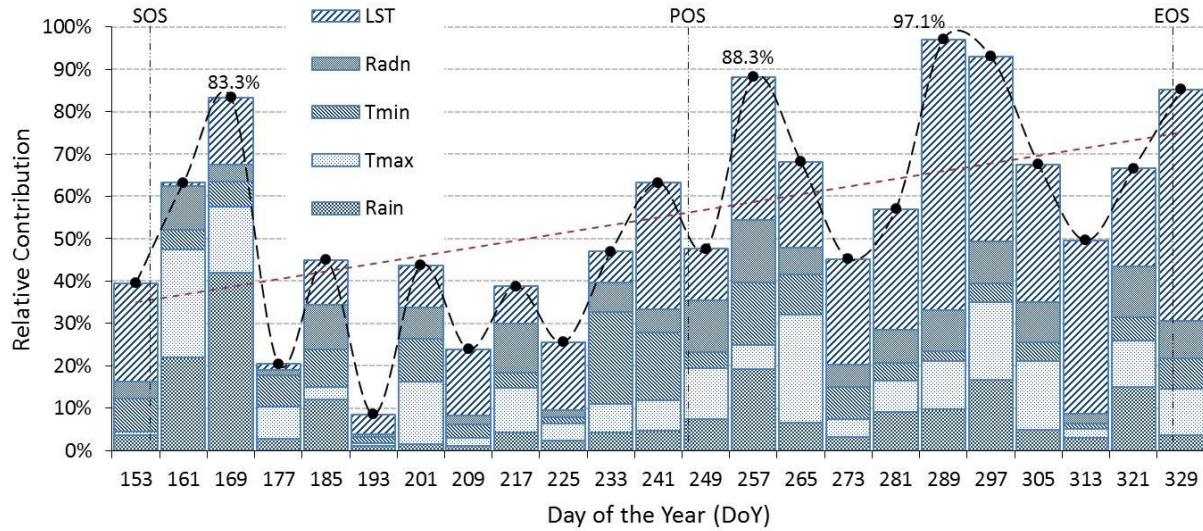
726 **Figure 5** Partial correlations between standardized anomalies (Sa-s) of 8-day EVI and individual

727 climate components in the growing seasons from 2001 to 2013. (a) rainfall; (b) maximum air

728 temperature and minimum air temperature; (c) land surface temperature; (d) radiation. Horizontal

729 dash lines: significance threshold where $p=0.05$. *: $p<0.1$, marginal significant. **: $p<0.05$,

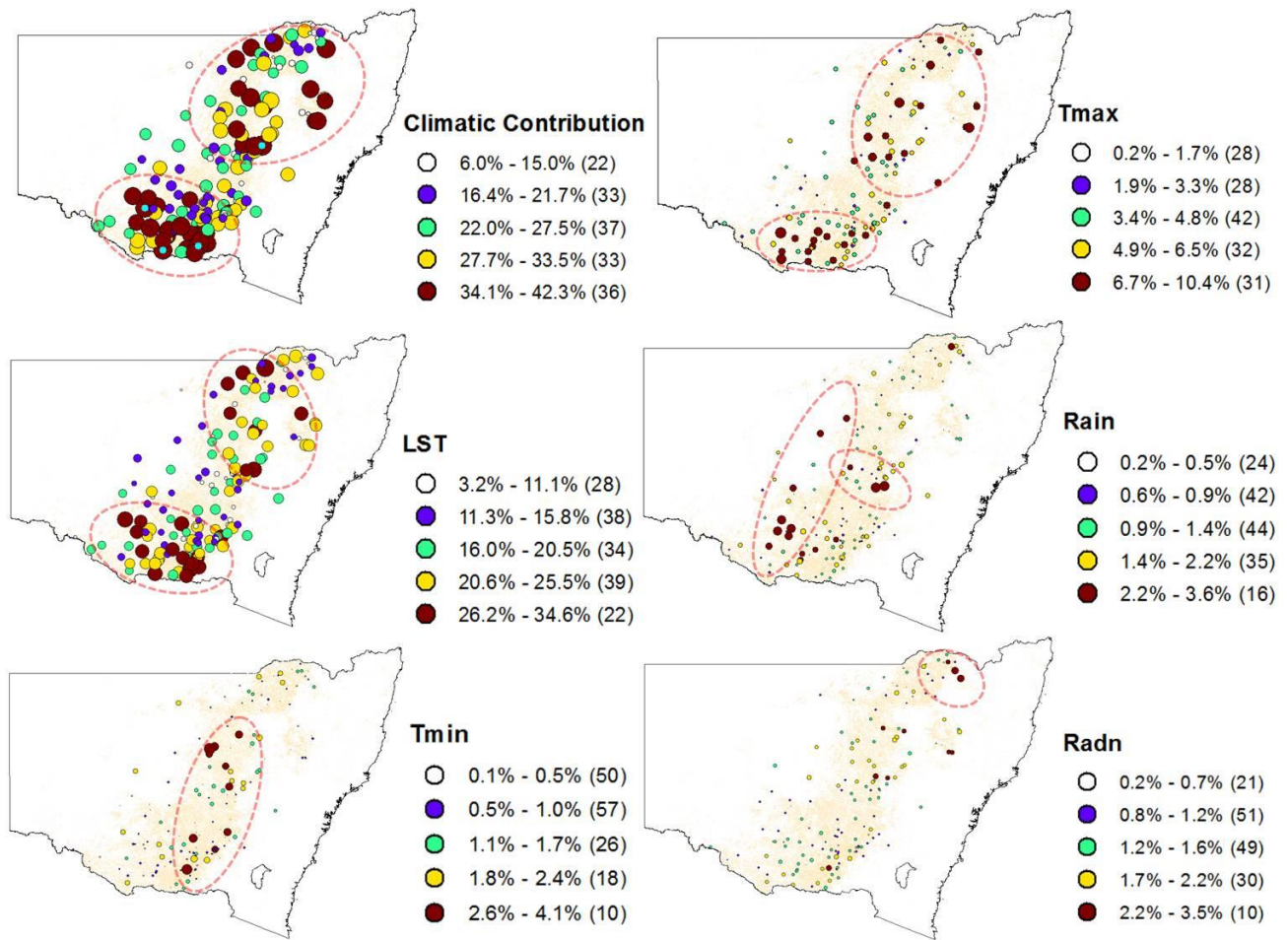
730 significant. X-axis: Date (Day of the Year)



732

733 **Figure 6** Individual and accumulated contributions of the climate and LST variability to the
 734 variation of EVI at the 8-day time scale in the growing season over 13 years. Stacked bars:
 735 individual contributions; black curve: accumulated contribution; brown dashed line: trend of
 736 accumulated contribution

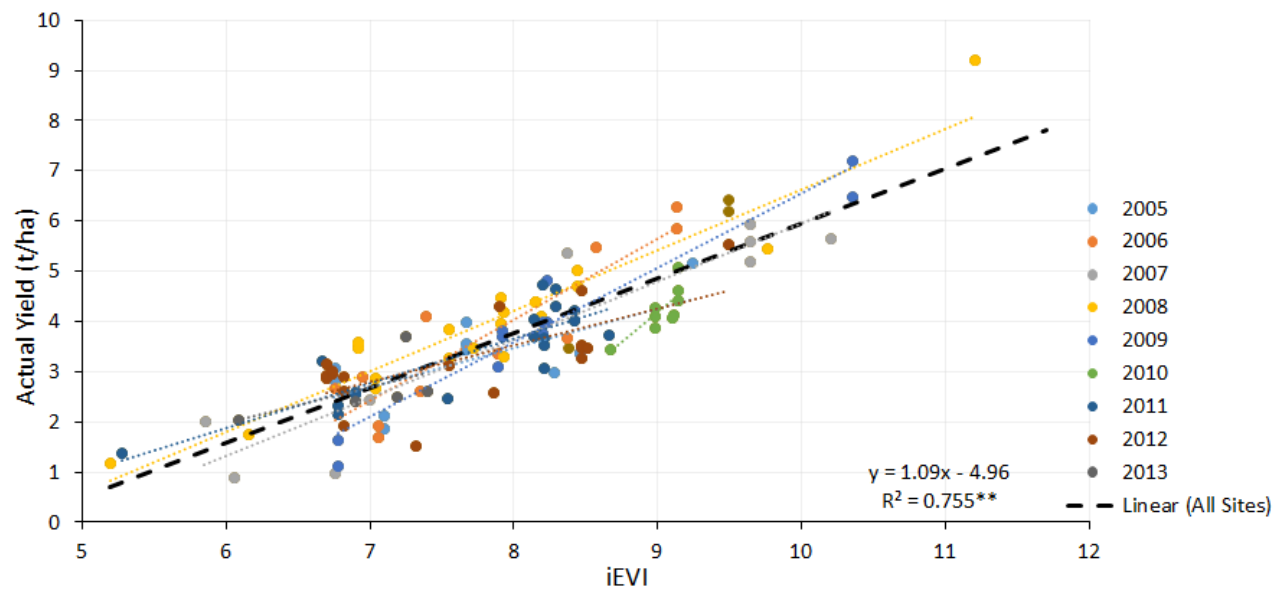
737



738

739 **Figure 7** Spatial distributions of the contributions of climate and LST standard anomalies (Sa-s)
 740 to EVI Sa-s in the growing season across the NSW cropland belts. Number in brackets: counts of
 741 tested pixels for which their attributes were in the corresponding range, and 161 pixels in total
 742 were tested

743



744

745 **Figure 8** Scatterplots between the actual yield and iEVI for 117 trial sites and their linear
 746 regression lines. **: p value < 0.001

747

748 TABLES

749

750 **Table 1** Seasonal climate and LST conditions each year across the rainfed cropland in NSW

	Pre-GS					VG					RG				
	Rain mm d ⁻¹	T _{max} °C	T _{min} °C	Radn MJ m ⁻²	LST °C	Rain mm d ⁻¹	T _{max} °C	T _{min} °C	Radn MJ m ⁻²	LST °C	Rain mm d ⁻¹	T _{max} °C	T _{min} °C	Radn MJ m ⁻²	LST °C
2001	1.18	28.91	14.06	20.31	32.51	1.16	16.80	3.91	11.81	15.63	1.29	23.64	9.24	20.85	30.32
2002	1.07	28.63	13.72	20.58	32.52	0.53	17.99	3.55	12.82	18.76	0.51	26.80	10.26	23.37	36.86
2003	1.07	28.61	14.83	20.37	33.61	1.46	16.48	4.57	11.81	15.75	1.07	23.49	8.59	21.93	30.12
2004	0.94	29.58	13.94	21.01	34.00	1.26	16.10	4.06	11.61	15.45	1.60	23.92	9.19	21.65	31.14
2005	0.62	29.22	13.65	21.15	34.06	1.87	16.84	4.98	11.80	15.87	2.16	24.25	10.43	20.72	27.99
2006	0.67	29.67	14.13	21.00	32.99	0.93	17.16	3.11	12.66	17.06	0.59	26.77	9.88	23.51	36.32
2007	1.15	29.67	15.53	20.36	34.47	0.95	16.50	4.00	12.19	16.47	0.83	26.18	10.35	22.11	34.58
2008	1.06	27.83	13.37	20.73	31.92	1.07	16.74	4.47	11.54	16.21	1.61	25.08	10.24	21.45	31.16
2009	1.03	28.98	14.50	20.62	33.38	1.05	17.27	5.22	11.45	16.29	0.80	26.71	10.92	21.48	33.91
2010	1.95	28.44	14.70	19.48	30.92	1.97	15.69	4.82	10.72	14.14	2.42	22.69	9.84	19.84	25.27
2011	1.69	27.80	13.81	19.33	28.80	0.83	17.52	4.00	11.83	16.60	1.73	24.80	9.96	20.59	29.65
2012	2.10	27.02	12.86	19.52	28.74	1.10	16.67	3.12	12.10	15.77	0.62	25.29	8.39	22.45	31.98
2013	1.08	29.17	14.11	20.71	33.14	1.28	17.81	5.17	11.60	16.91	0.76	26.28	9.19	23.10	33.15
Mean	1.20	28.73	14.09	20.40	32.39	1.19	16.89	4.23	11.84	16.22	1.23	25.07	9.73	21.77	31.73
Sd	0.43	0.77	0.66	0.58	1.79	0.38	0.63	0.69	0.51	1.03	0.60	1.35	0.73	1.08	3.13

751 * Pre-GS was calculated as the period from the first day of the year to Start of Season (SOS) at day 156. Sd is one standard deviation

752 in each crop growth stage from 2001 to 2013. Red, yellow and green correspond to the order of the variable values from high to low

753 among the pre-growing season (Pre-GS), vegetative growth phase (VG) and reproductive growth phase (RG)

754